Thermal resistance field estimations from IR thermography using multiscale Bayesian inference

M. M. Groz, A. Sommier, E Abisset-Chavanne, S. Chevalier, J. L. Battaglia, J. C. Batsale, Christophe Pradere

Thermal resistance field estimations from IR thermography using multiscale Bayesian inference

M.M. Groz[a], A. Sommier[b], E. Abisset-Chavanne[b], S. Chevalier[b], J.L. Battaglia[b], J.C. Batsale[b] and C. Pradere[b,1]

[a] Epsilon-Alcen, Esplanade des arts et métiers, 33405 Talence Cedex, France.
[b] I2M UMR CNRS-UB-ENSAM 5295, Esplanade des arts et métiers, 33405 Talence Cedex, France.

Abstract

The main goal of this paper is the estimation of thermal resistive fields in multilayer samples using the classical front face flash method as excitation and InfRared Thermography (IRT) as a monitoring sensor. The complete inverse processing of a multilayer analytical model can be difficult due to a lack of sensitivity to certain parameters (layer thickness, depth of thermal resistance, etc.) or processing time. For these reasons, our present strategy proposes a Bayesian inference approach. Using the analytical quadrupole method, a reference model can be calculated for a set of parameters. Then, the Bayesian probabilistic method is used to determine the maximum likelihood probability between the measured data and the reference model. To keep the processing method robust and fast, an automatic selection of the calculation range is proposed. Finally, in the case of a bilayer sample, both the thickness and resistive 3D layers are estimated in less than 2 min for a space and time matrix of 50000 pixels by 4000 time steps with a reasonable relative error of less than 5%.

1 Introduction

This work is a continuity study by our team on the development of quantitative methods for thermal resistance field characterization. Thus, as presented in [1], in the field of Quantitative InfraRed Thermography (QIRT), Non Destructive Testing (NDT) methods are very widespread for the detection of defaults, whereas few techniques are completely quantitative. In fact, many authors have developed techniques for qualitative in-depth defect detection using flash thermography, the Thermal Signal Reconstruction (TSR) technique [2, 3] or the lock-in technique [4]. Moreover, [5] and [6] linked the TSR method with the quantitative estimation of defect depth. A similar study was performed by[7] with a technique based on Pulsed Phase Transformation (PPT) and thermographic signal reconstruction [8]. Similarly, these methods are often applied in techniques stemming from measurements of monosensors and minimization by nonlinear methods. For example , the Markov chain Monte Carlo method has been implemented within the picosecond time-resolved technique to estimate the thermal resistance at the interface between thin films at high temperatures [9, 10]. In addition, the Levenberg-Marquardt minimization technique has been use to estimate the thermal resistance between thin films from measurements collected using either the thermoreflectance technique [11] or modulated photothermal radiometry within the infrared spectrum [12]. Adapting these inverse methods to field methods becomes very time consuming. Thus, our main objective is to develop rapid and quantitative methods. [1] was based on an asymptotic development with a quantitative and fast computational approach that does not allow for the estimation of several resistive layers. To extend the applicability of these approaches, we propose the implementation of Bayesian-type methods. comparing this study with a prior study [1]based on asymptotic method, we can highlight that in this sample case, the Bayesian approach allows for the estimation of more parameters. In fact, the knowledge of delamination and more particularly of Rth is of crucial interest for material health as well as the possibility of calculating a heat balance on materials subjected to high flows such as composite materials but more recently materials from additive manufacturing processes for example. In this work, a flash setup is used, and then, the methods, including several components, are developed to introduce the direct modeling of multilayer samples using a quadrupole formulation. Then, in the inverse processing section, the Bayesian inference is presented, and finally, in the results and discussion section, the method is validated on the same sample used in [1] to compare both approaches.

2 Materials and Measurements

In this paper, the same classical front face flash method setup, as illustrated in [1], is used for the measurements. To briefly describe the setup, the flash lamp comes from

Uniblitz and has an energy E of 1600 J. The lamp is synchronized with the IR camera by using an analogical TTL link to perform a pre-trigger mode before the flash. The IR camera is an MCT long-wave (λ = 9–11 µm) FLIR SC7600 with a matrix sensor of 320 × 256 pixels and a pitch of 30 × 30 µm^2. With the used lenses and the sample distance, the resulting spatial resolution is approximately 300 × 300 µm^2 per pixel. A homemade (as illustrated in figure 1) reference sample was used to calibrate the depth and thickness of the thermal resistance represented by an air square hole. The geometrical and thermal properties are reported in figure 1.a. In this case, only a bilayer was designed to demonstrate the capacity of the proposed method. Moreover the polycarbonate front face was black painted to guarantee a surfacic absorption of the flash lamp heat flux and uniform temperature measurement of the IR camera. The goal of the Bayesian approach is to estimate the fields of the two resistive layers as well as the thickness variation of the polycarbonate layer located between these layers. For all reference samples in figure 1, it is important to note that the minimum tolerance guarantee by the supplier is approximately +50 μm for the designed thickness.

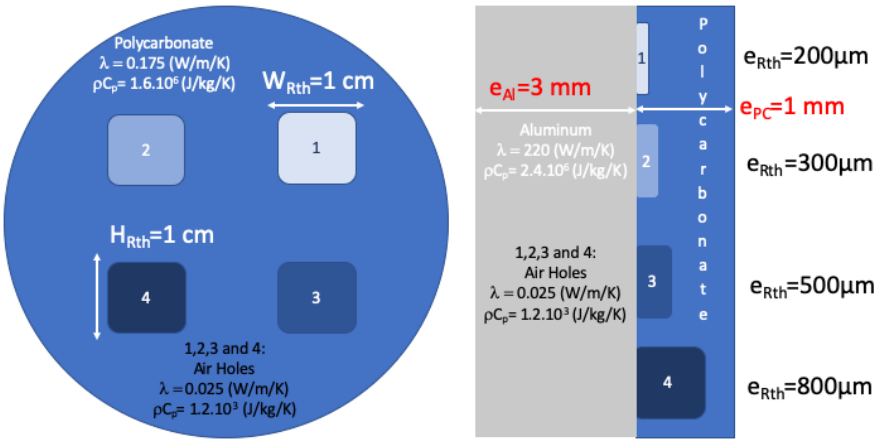

Fig. 1: Schematic of the reference monoresistive layer sample used in [1]

3 Principle of the proposed methods

3.1 Direct Problem

Using the quadrupole formulation [13], the thermal response of any assembly can be generalized according to equation 1. The quadrupole method enables many layers as well as thermal resistances to be accounted for. A MatLab homemade application (https://fr.mathworks.com/matlabcentral/fileexchange/74199-1dt-multilayer-thermal-quadrupole-solver-and-builder) was developed to generate any assembly and also to

realize the sensitivity analysis [14, 15] to all parameters of the multilayer. The model can be expressed as follows:

$$\begin{bmatrix} \theta_0(p) \\ \phi_0(p) - h\theta_0(p) \end{bmatrix} = \left[\prod_{i=1}^{N} M_1 R_1 ... R_{i-1} M_i R_i ... R_{N-1} M_N\right] \begin{bmatrix} \theta_e(p) \\ h\theta_e(p) \end{bmatrix} \tag{1}$$

where θ_0 (K) and θ_e (K) represent the Laplace transforms of the front $(z = 0)$ and rear $(z = e)$ face temperature, respectively, in each pixel composing the temperature fields; h $(W.m^{-2}.K^{-1})$ is the convective heat loss; and $\phi_0(p)$ $(W.m^{-2})$ is the Laplace transform of the heat flux at the front face. The heat flux waveform can be represented by a Dirac function, a Heaviside function or a pulse with a duration linked to the flash lamp discharge time. Finally, M_i is the matrix relative to layer i, and R_i is associated with the thermal resistance between layers i and $i + 1$, expressed as follows:

$$\begin{cases} M_i = \begin{bmatrix} \cosh\left(\sqrt{\frac{p}{a_i}} e_i\right) & \frac{\sinh\left(\sqrt{\frac{p}{a_i}} e_i\right)}{\sqrt{\frac{p}{a_i}} \lambda_i} \\ \sqrt{\frac{p}{a_i}} \lambda_i \sinh\left(\sqrt{\frac{p}{a_i}} e_i\right) & \cosh\left(\sqrt{\frac{p}{a_i}} e_i\right) \end{bmatrix} \\ R_i = \begin{bmatrix} 1 & Rth_i = \frac{e_i}{\lambda_i} \\ 0 & 1 \end{bmatrix} \end{cases} \tag{2}$$

where p (s^{-1}) is the Laplace variable, e_i (m) is the thickness of layer i, a_i $(m^2.s^{-1})$ is the thermal diffusivity of layer i, λ_i $(W.m^{-1}.K^{-1})$ is the thermal conductivity, and Rth_i $(m^2.K.W^{-1})$ is the interfacial thermal resistance. All of these parameters are collected in the variable $\boldsymbol{\beta}$. Finally, from the solutions to equations 1 and 2 expressed in the Laplace domain, the 1D transient analytical front face temperature $T_0(t, \boldsymbol{\beta})$ can be calculated using the Stehfest algorithm [16] for any assembly characterized by the variable $\boldsymbol{\beta}$.

In the following, and without a loss of generality, a unique thermal resistance is considered in the thickness of the sample. Then, the variable $\boldsymbol{\beta}$ is reduced to the couple $[e, Rth]$.

3.2 Inverse processing method based on Bayesian inference

To reconstruct the sample, the inverse problem can now be defined in each pixel of the image as follows: knowing the measured temperature evolution $T_e(t)$ at $z = 0$ (front face), we can determine the polycarbonate thickness e_{PC} and thermal resistance magnitude Rth, *i.e.*, the couple $\beta = [e_{PC}, Rth]$.

To do so, it is proposed to use Bayesian inference, a probabilistic method based on the Bayes relations [17]:

$$\pi_{posterior}(\boldsymbol{\beta}|T_0(t)) = \frac{\pi(T_0(t)|\boldsymbol{\beta}) \cdot \pi_{prior}(\boldsymbol{\beta})}{\pi(T_0(t))} \tag{3}$$

where $\pi_{posterior}(\boldsymbol{\beta}|T_0(t))$ is the posterior probability density, i.e., the conditional probability of $\boldsymbol{\beta}$, given the measured front face temperature $T_0(t)$; $\pi_{prior}(\boldsymbol{\beta})$ is the prior density, which is the a priori information about $\boldsymbol{\beta}$ prior to the measurements; $\pi(T_0(t)|\boldsymbol{\beta})$ is the likelihood function, which expresses the likelihood of different temperature measurement outcomes $T_0(t)$ with $\boldsymbol{\beta}$ given; and $\pi(T_0(t))$ is the model evidence or the marginal probability density of the measurements, which plays the role of a normalizing constant.
Bayesian inference is then a stochastic approach that results in a probability density function providing a probability weight to each possible variable $\boldsymbol{\beta}$.

In the first stage, the evidence is not considered. Indeed, even if its computation does not represent a tricky issue due to the analytical nature of the direct problem, the knowledge of the more probable $\boldsymbol{\beta}$ in each pixel, independent of the normalization, is sufficient to reconstruct the thickness composition. For the prior, which allows us to account for the *a priori* knowledge of $\boldsymbol{\beta}$, only a limitation of the parametric space (e_{PC}, Rth) in the variation range of the parameters is considered to be as general as possible. Then, the prior is taken as a uniform probability of the variation range of each parameter $[e_{PCmin}, e_{PCmax}]$ and $[Rth_{min}, Rth_{max}]$ with a null probability outside.

Then, finally, in our case, the posterior probability density is directly linked to the likelihood function [18]:

$$\pi_{posterior}(\boldsymbol{\beta}|T_0(t)) \propto \pi(T_0(t)|\boldsymbol{\beta}), \boldsymbol{\beta} \in [e_{PCmin}, e_{PCmax}] \times [Rth_{min}, Rth_{max}] \tag{4}$$

The likelihood function $\pi(T_0(t)|\boldsymbol{\beta})$ is defined as follows:

$$\pi(T_0(t)|\boldsymbol{\beta}) \propto \exp\left(-\frac{1}{2\Gamma^2}||T_M(t) - T_0(t,\boldsymbol{\beta})||_2^2\right), \tag{5}$$

where $T_0(t,\boldsymbol{\beta})$ is the estimated front face temperature computed using the direct model defined in Section 3.1 for $\boldsymbol{\beta} \in [e_{PCmin}, e_{PCmax}] \times [Rth_{min}, Rth_{max}]$, and $T_M(t)$ is the measured front face temperature at each pixel.

In this case, as the forward problem is analytical and few parameters are considered, the likelihood function is built by directly sampling the discretized parametric space (e_{PC}, Rth). This allows us to not have to rely on Markov chain Monte Carlo methods, which are commonly used when the large computation time of the forward problem

prevents the exploration of the entire parameter space [18, 19, 20, 21]. This also allows for defining an iterative multiscale refinement of the parametric space function of the sample parameter heterogeneity, as presented in Section 4.

4 Results and Discussion

In this section, the method presented in the previous section is detailed through the following results based on the bilayer presented in figure 1. The main idea of the proposed method is to obtain a complete automatic estimation of the sample properties. To do so, the following steps are performed: (i) a coarse grid of the parameter space is defined, (ii) the inverse processing 5 is performed, (iii) a segmentation process is performed to identify the sample heterogeneity and segment it in several ROIs, (iv) a fine parameter grid is defined, and (v) this is used to realize the final inverse processing.
First, by using the front face flash setup, the sample is measured according to the following parameters: (i) flash duration of 1 ms, (ii) camera frequency acquisition of 200 Hz, and (iii) 4000 images corresponding to a final time of 20 s and a spatial resolution of $300 \times 300\ \mu m^2$ per pixel. The obtained results are plotted in figure 2.

a) b)

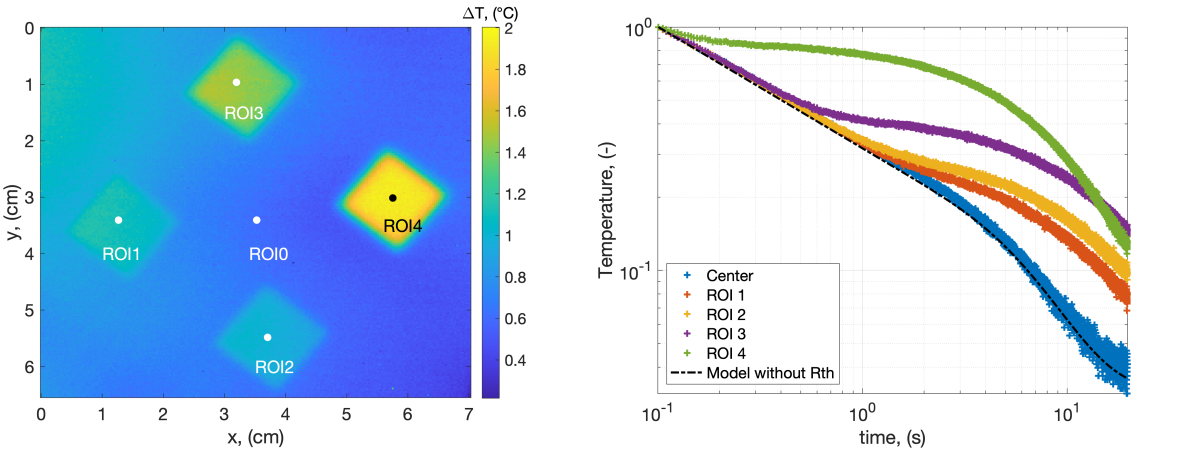

Fig. 2: a) Measured temperature field at $t = 5.12$ s after the flash and b) dimensionless temperature response of the front face of the different ROIs (point located in figure 2.a). The measurements properties are a pulse of 1 ms duration. Whereas dimensionless analytical solution are calculated from the estimated value (solid line) of the table 1 and without thermal resistance (dash line)

.

In figure 2.b, the dimensionless temperature comes from the following formulation: $T_0^*(t) = \dfrac{T^c(t \geq t_{ref})}{T^c(t_{ref})}$, with $T^c(t) = T_0(t) - T_0(t \leq t_0)$, $t_0(s)$ being the starting time of the flash, and $t_{ref}(s)$ being the reference time for the normalization with a -1/2 slope.

One can observed that depending on the thermal resistance depth and magnitude, the temperature moves away from the -1/2 reference slope. Moreover in the figure 2.b, from the final estimated interval data of each ROIs reported in the table 1, the exact dimensionless analytical model was calculated and superposed with the experimental dimensionless measurements.

From the measurements, a first estimation is performed for (i) variation range of layer 1 thickness (*i.e.*, polycarbonate) $e_{PC} = [50, 950]\ \mu m$ and (ii) corresponding thermal resistance thickness $e_{Rth} = [50, 950]\ \mu m$ with a thermal conductivity value of $\lambda_{air} = 0.025\ W.m^{-1}.K^{-1}$ to give the final generated thermal resistance variation range $Rth_g = [0.0020, 0.038]\ m^2.K.W^{-1}$. Using these variation ranges, one can then build the 2D parametric space needed for the Bayesian inference method by discretizing the variation range of depth e_{PC} and thermal resistance Rth.

In the first attempt, a coarse discretization of 10 nodes per parameter is considered, which corresponds to a discretization step of 100 μm for the depth and 0.004 $m^2.K.W^{-1}$ for the thermal resistance. The parametric space can then be filled by computing the temperature $T_0(t, \boldsymbol{\beta})$ for the 11×11 possible combinations of the parameters defining $\boldsymbol{\beta}$. The complete calculation of such a base takes 0.6 s on a 2.3 GHz quad-core i5 laptop with 16 GHz of RAM.

The likelihood is then computed from equation 5. For each couple of parameters, a maximum probability corresponding to the minimum likelihood deviation is obtained for each pixel (see figure 3.a). From this couple, the maximum can be reported for the entire image, as depicted in figure 3.b.

a) b)

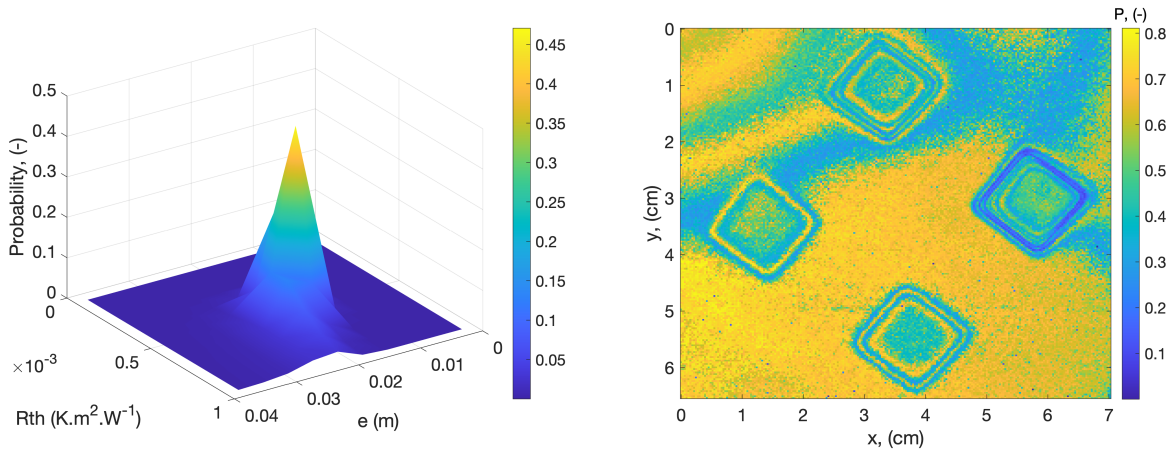

Fig. 3: a) Calculated fields of Bayesian probability for the pixel located on $x = 3.5$ cm and $y = 1$ cm in figure 2.a and b) estimated probability field for all measurement data in figure 2.

From the location of this maximum probability, the corresponding couple of parameters (see figure 3.a) can be extracted for each pixel giving the reconstructed images of figure 4. In figure 3.b, the decreases in the probability around the resistive square hole are linked to the 3D effects of the thermal diffusion that are not taken into account in the proposed 1D model. As a consequence, the probability can also indicate a model error.

a) b)

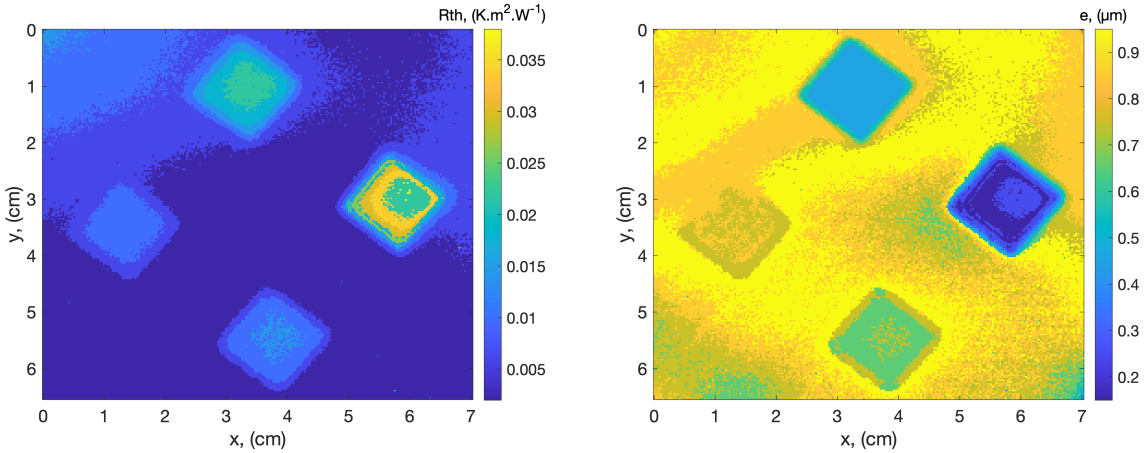

Fig. 4: Estimated fields for a coarse mesh of a) thermal resistance Rth $(m^2.K.W^{-1})$ *and b) polycarbonate layer thickness* e_{PC} (m).

This first calculation for the entire measurement matrix take 66 s on a 2.3 GHz quad-core i5 laptop with 16 GHz of RAM. Due to the size of the measured images and acquisition time, the space and time dimensions are (i) 51012 pixels corresponding to 218 x 234 pixels along the x and y directions and (ii) 4000 time steps.

From the estimated field of thermal resistance in figure 4.a, the image is segmented into several regions (see figure 5.a) using the [22] method. In the present case, 5 ROIs are obtained relative to the 4 thermal resistances and one background (ROI0) linked with the contact defect between the polycarbonate (as illustrated figures 2.a and 5.a) and aluminum plate. From this ROI and using the probability level in figure 3.b, each area can be optimized by keeping the values greater than 0.6 as presented in the figure 5.b where the higher value are reported.

From this segmentation, a second refined grid in the parametric space can be defined, as illustrated in figure 5.c. In this figure, the complete methodology is summarized. To increase the visibility of figure 5.c, the background ROI behavior (0 in figure 5.a) is not reported.

a) b)

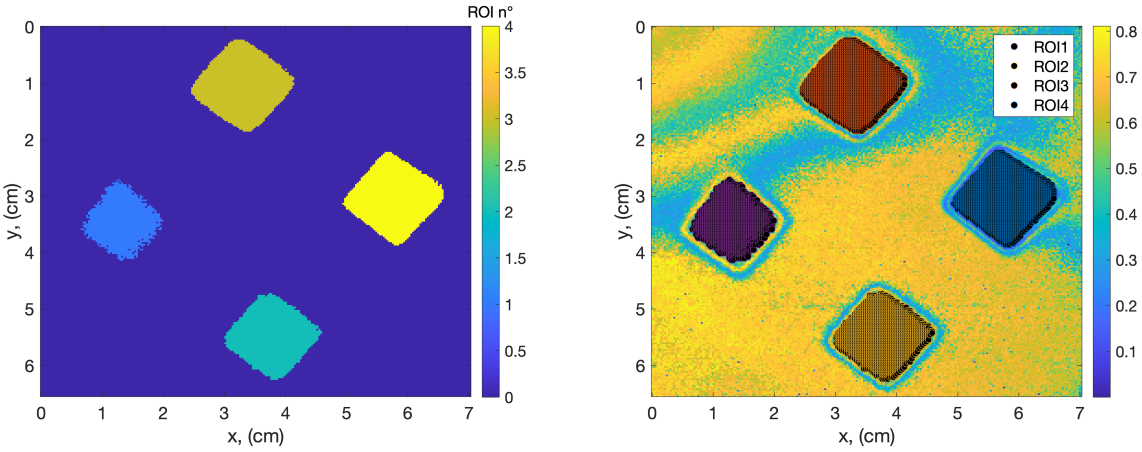

c)

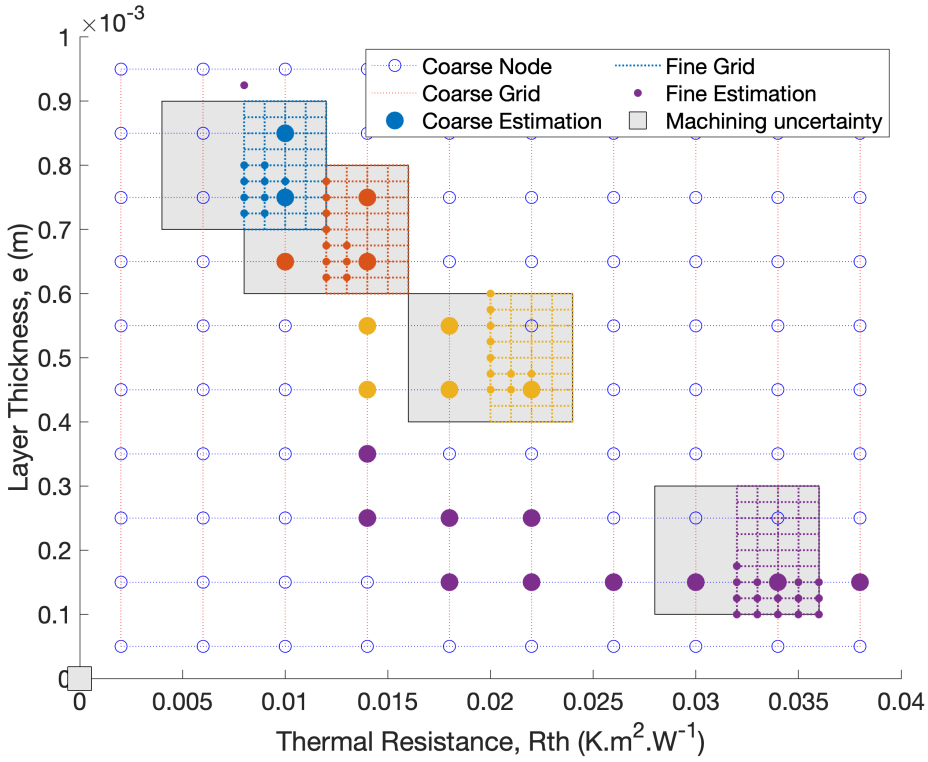

Fig. 5: a) Labeling of the heterogeneity of the sample in terms of the ROI, b) selection of the probability higher than 0.6 in each ROIs and c) synthesis of the mesh composed of several parameters and estimated area as function of the different ROIs.

Furthermore, a parameter minimum step was chosen, i.e., $\delta Rth = 0.001$ and $\delta e_{PC} = 25\mu m$, to recalculate a new refined analytical database. The corresponding fine grid is reported in table 1. In this database, Bayesian inference can be applied and the couple of maximum probability linked with the fine mesh (or parameter space) of each ROI is reported using the small dots. From the probabilistic processing, the complete parameters are reported in figure 6 according to the fine grid of each ROI or sample heterogeneity.

a) b)

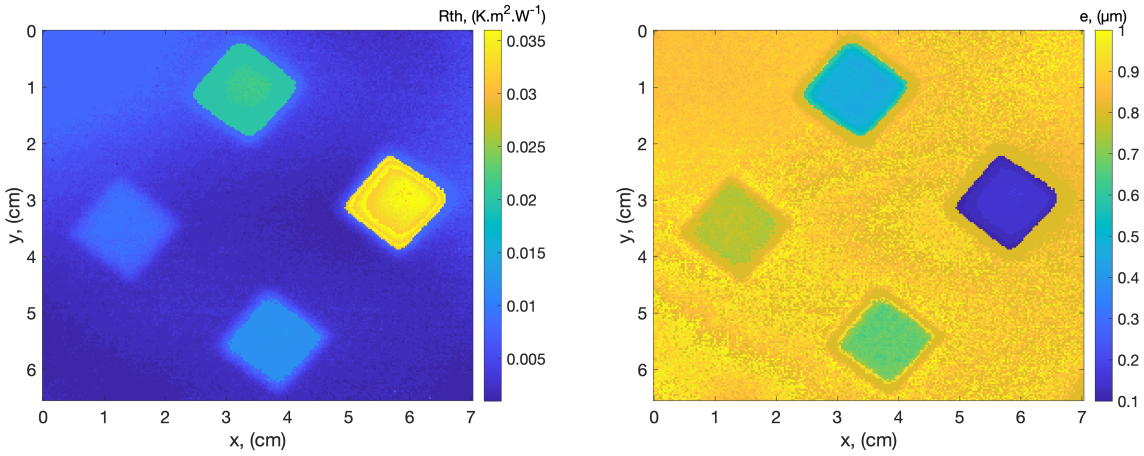

Fig. 6: Estimated fields for a fine mesh of a) thermal resistance $Rth(m^2.K.W^{-1})$ and b) polycarbonate layer thickness e_{PC} (m).

The exact CPU times are reported in table 1. It is important to note that the calculation process of each ROI is approximately 0.2 s for the ROI database and 2 s for the Bayesian processing, which is mainly linked to the number of pixels in the ROIs.

	e_{PC} ** (μm)	e_{Rth} ** (μm)	Pixel number (-)	Bayesian method CPU time (s)	Database CPU time (s)
Complete image	[50:100:950]	[50:100:950]	51012	66	0.32
*ROI 0	[800:25:1000]	[25:25:200]	44583	44	0.23
*ROI 1	[700:25:900]	[200:25:250]	1207	1.2	0.75
*ROI 2	[600:25:800]	[300:25:350]	1612	1.4	0.13
*ROI 3	[400:25:600]	[500:25:550]	1856	1.7	0.13
*ROI 4	[100:25:300]	[800:25:850]	1754	1.6	0.12
*, The ROI order can be found in the figures 2.a and 5.a					
**, Systematic maximum machining uncertainty of +50 μm given by the supplier; see section 2					

Tab. 1: Calculation time comparison as function of the number of pixels and parameter base size.

Finally, from the fine maps of both parameters (R_{th} and e_{PC}), the 3D topology of the polycarbonate layer thickness and thermal resistance deepness are reported in figure 7.

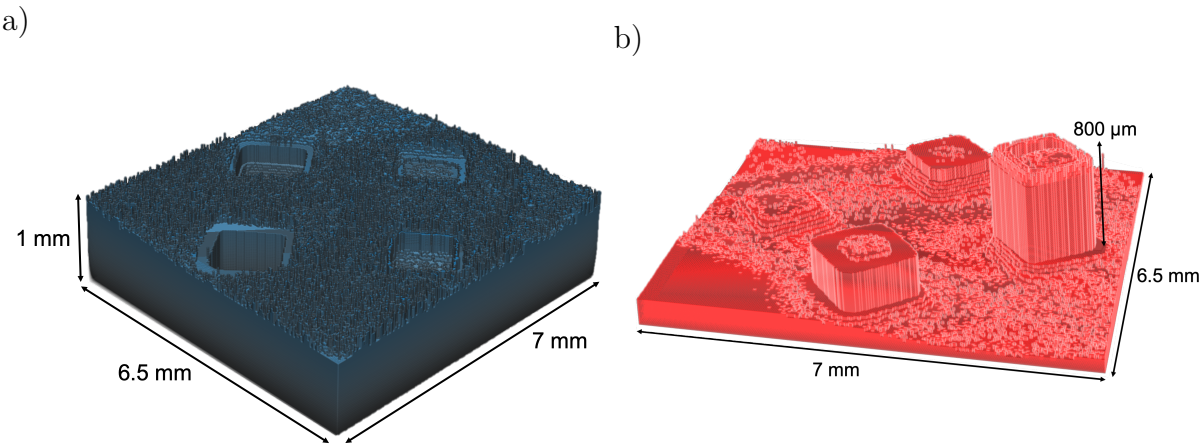

Fig. 7: Reconstructed 3D fields of a) the polycarbonate thickness layer and b) thermal resistive layer assimilated to air thickness.

One can observed that in figure 7.a, the polycarbonate layer is in very good agreement with the machining sample shape shown in figure 1. The 3D map in figure 7.b represents the shape of the air layer inside the complete assembly. This representation can be assembled to form the complete 3D topology of the sample which demonstrates the use of thermal tomography of the bilayer heterogeneous sample from IRT surface measurements using flash excitation.

From the estimated parameters fields represented figure 6, the measured temperatures (figure 2) are plotted and superposed with the model recalculated for the pixels of the different ROIs (see figure 2) as illustrated in the figure 8.a. Then, the residual are reported in the figure 8.b. They are expressed according to the following expression $res = 100 * (1 - \frac{T_{mes}}{T_{model}})$ with T_{mes}, the measured temperature and T_{model}, the calculated temperature. It is interesting to notice that the error are very low excepted for the ROI4 where a bias appeared at the short time. This gap is mostly due to the normalisation that cannot be correctly done due to the lack of short time measurements. As a consequence a bias occurred, nevertheless the error is around 10%. Finally, to quantitatively analyse the uncertainty of Bayesian approaches, the sum of the estimated thickness of the bilayer is calculated and presented in figure 8.c. In figure 8.d, the relative error, based on the theoretical well-known polycarbonate layer thickness of 1 mm, is calculated. The maximal uncertainty reaches 15% with an average value of 3.15%, which is very acceptable for the complete measurement, inversion and reconstruction processing. This maximal uncertainty is mainly located in the background ROI and close to the boundary of the thermal resistance ROIs. For the background, the explanation comes from the depth, which causes a decreases in the method sensitivity. However, close to the interface of the resistive square hole, the explanation comes from the 1D model used as a direct model in Bayesian inference, whereas 3D heat transfer is predominant close to the sample interface.

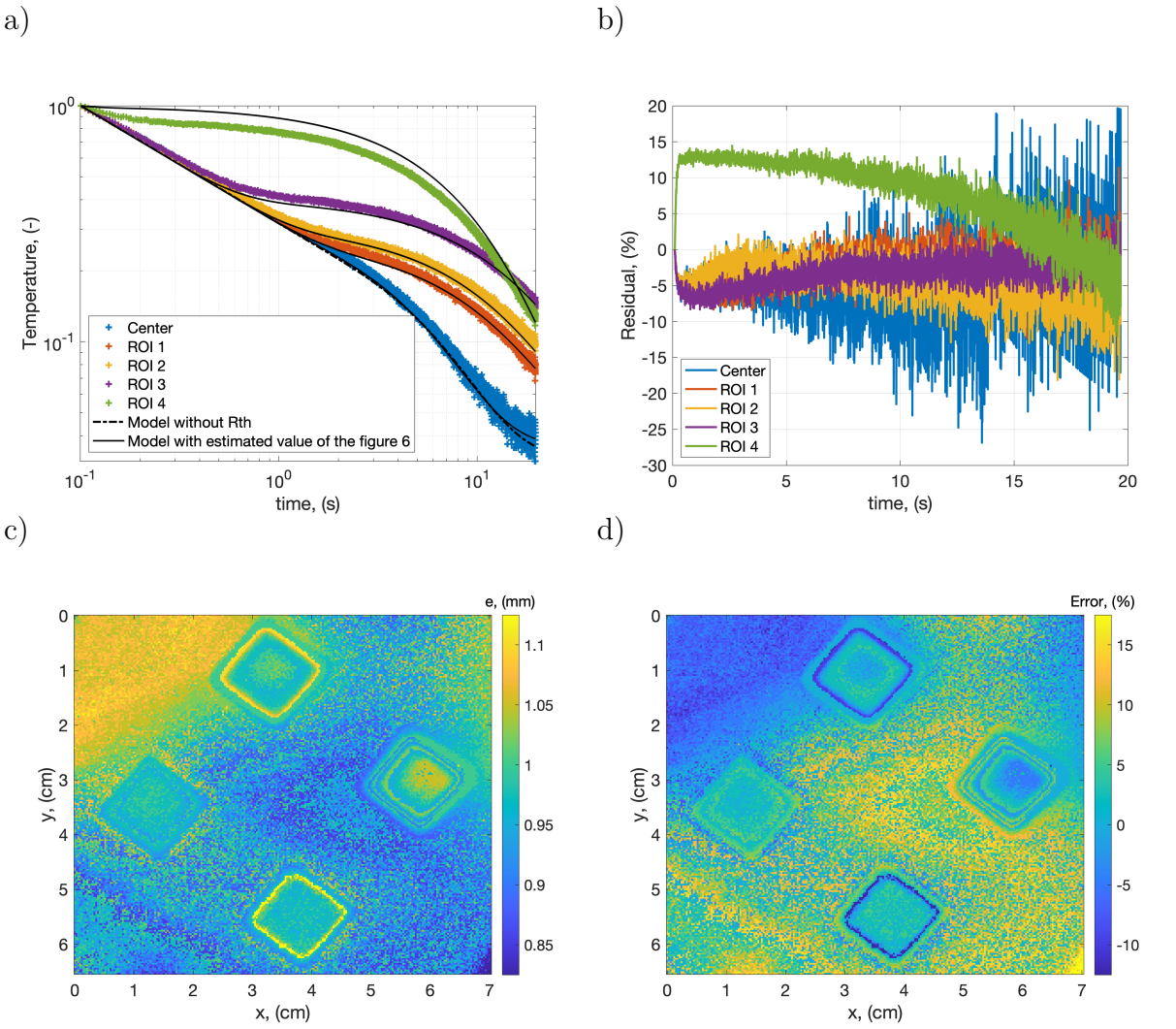

Fig. 8: a) Recalculated temperature by using the model of the equation 1 with the estimated value of the figure 6 for the measured temperature of the figure 2, b) Residual calculated between the measurement and the model according to the following formulation $100 * (1 - \frac{T_{mes}}{T_{model}})$ *with* T_{mes} *(dash line) the measured temperature and* T_{model} *(solid line) the calculated temperature with estimated parameters , c) Recalculated total thickness from the estimated polycarbonate and resistive layers and d) relative error calculated for a thickness value of 1 mm measured after machining.*

5 Conclusions

In this paper, a methodology for both quantitative thermal resistance and layer thickness imaging estimation is proposed. This method is based on the Bayesian inference probabilistic inverse method and the analytic quadrupole solution of the thermal response to front face flash excitation of a bilayer assembly using measured IRT temperatures. The main advantages of this method are as follows: (i) the possibility to handle any type of multilayer (high number of layers), (ii) the fast inverse processing that can be adapted for online monitoring (inverse processing in less than 2 min), and (iii) the ability of the

method to overcome the knowledge of the initial excitation heat flux as well as the absolute measured temperature and the capacity to retrieve 3D mapping of the layer thickness. However, the main drawbacks of the proposed methods are as follows: (i) the 1D character of the model can cause blurring close to the interface, and (ii) the sensitivity to the sample parameters depends on the thermal contrast of the layers. Finally, comparing this study with a prior study [1] based on asymptotic method, we can conclude that in this sample case, the Bayesian approach allows for the estimation of more parameters (polycarbonate layer plus thermal resistance). Moreover, the two methods can be used together, especially the asymptotic one, to quickly retrieve the thermal resistive layer, which can be refined using the Bayesian inference method.

Acknowledgment

The authors would like to thank the "nouvelle aquitaine" for the financial support of the regional project THIRUS.

References

[1] Groz, M.-M. *et al.* Estimation of thermal resistance field in layered materials by analytical asymptotic method. *Applied Sciences* **10**, 2351 (2020). 2, 3, 13

[2] Shepard, S. M. Flash thermography of aerospace composites. In *IV Conferencia Panamericana de END Buenos Aires*, vol. 7 (2007). 2

[3] Balageas, D., Chapuis, B., Deban, G. & Passilly, F. Improvement of the detection of defects by pulse thermography thanks to the tsr approach in the case of a smart composite repair patch. *Quantitative InfraRed Thermography Journal* **7**, 167–187 (2010). 2

[4] Karpen, W., Wu, D., Steegmuller, R. & Busse, G. Depth profiling of orientation in laminates with local lockin thermography. In *Proc. QIRT*, vol. 94, 23–26 (1994). 2

[5] Oswald-Tranta, B., Maier, A. & Schledjewski, R. Defect depth determination in a cfrp structure using tsr technique. *The* **12** (2014). 2

[6] Roche, J.-M. & Balageas, D. Imagerie quantitative tsr-rvb: de la détection de défauts au d-scan thermique . 2

[7] Ibarra-Castanedo, C. & Maldague, X. Pulsed phase thermography reviewed. *Quantitative Infrared Thermography Journal* **1**, 47–70 (2004). 2

[8] Shepard, S. M., Lhota, J. R., Rubadeux, B. A., Wang, D. & Ahmed, T. Reconstruction and enhancement of active thermographic image sequences. *Optical Engineering* **42**, 1337–1343 (2003). 2

[9] Nóbrega, P. H. A., Orlande, H. R. & Battaglia, J.-L. Bayesian estimation of thermophysical parameters of thin metal films heated by fast laser pulses. *International communications in heat and mass transfer* **38**, 1172–1177 (2011). 2

[10] Battaglia, J.-L. *et al.* Identification of the temperature-dependent thermal boundary resistance at a metal-phase change material. *Inverse Problems in Science and Engineering* **20**, 941–950 (2012). 2

[11] Battaglia, J.-L. *et al.* Thermal resistance at al-ge2sb2te5 interface. *Applied Physics Letters* **102**, 181907 (2013). 2

[12] Battaglia, J.-L. *et al.* Thermal characterization of the si o 2-ge 2 sb 2 te 5 interface from room temperature up to 400 c. *Journal of Applied Physics* **107**, 044314 (2010). 2

[13] Maillet, D. *Thermal quadrupoles: solving the heat equation through integral transforms* (John Wiley & Sons Inc, 2000). 3

[14] Pech-May, N. W., Mendioroz, A. & Salazar, A. Generalizing the flash technique in the front-face configuration to measure the thermal diffusivity of semitransparent solids. *Review of Scientific Instruments* **85**, 104902 (2014). 4

[15] Bernegger, R., Altenburg, S. & Maierhofer, C. Quantification of delaminations in semitransparent solids using pulsed thermography and mathematical 1d models. *International Journal of Thermophysics* **41**, 1–19 (2020). 4

[16] Stehfest, H. Algorithm 368: Numerical inversion of laplace transforms [d5]. *Communications of the ACM* **13**, 47–49 (1970). 4

[17] Bayes, T. An essay towards solving a problem in the doctrine of chances. 1763. *MD computing: computers in medical practice* **8**, 157 (1991). 5

[18] Kaipio, J. & Somersalo, E. *Statistical and computational inverse problems*, vol. 160, 49–112 (Springer Science & Business Media, 2006). 5, 6

[19] Carlin, B. P. & Chib, S. Bayesian model choice via markov chain monte carlo methods. *Journal of the Royal Statistical Society: Series B (Methodological)* **57**, 473–484 (1995). 6

[20] Metropolis, N., Rosenbluth, A. W., Rosenbluth, M. N., Teller, A. H. & Teller, E. Equation of state calculations by fast computing machines. *The journal of chemical physics* **21**, 1087–1092 (1953). 6

[21] Derin, H., Elliott, H., Cristi, R. & Geman, D. Bayes smoothing algorithms for segmentation of binary images modeled by markov random fields. *IEEE Transactions on Pattern Analysis and Machine Intelligence* 707–720 (1984). 6

[22] Otsu, N. A threshold selection method from gray-level histograms. *IEEE transactions on systems, man, and cybernetics* **9**, 62–66 (1979). 8